RSC Advances

PAPER

View Article Online
View Journal | View Issue

Cite this: *RSC Adv.*, 2020, **10**, 32113

A novel viewpoint of an imidazole derivative ionic liquid as an additive for cobalt and nickel electrodeposition†

Inam M. A. Omar,[ab] Khadijah M. Emran,[*b] Madzlan Aziz[a] and Abdo M. Al-Fakih[a]

Thin films of Co and Ni electroplated onto a copper electrode from acidic sulfate and Watts baths, respectively, were investigated. The use of an ionic liquid additive in the electrolyte is widespread for producing thin films by electrodeposition. In the present work, the influence of a new ionic liquid, namely, 1-methyl-3-((2-oxo-2-(2,4,5-trifluorophenyl)amino)ethyl)-1*H*-imidazol-3-ium iodide (Im-IL), in the electrodeposition of two metals was investigated using cathodic polarization (CP), cyclic voltammetry (CV), and anodic linear stripping voltammetry (ALSV) measurements and cathodic current efficiency (CCE%). The surface morphology of the Co- and Ni-coated samples was examined using Scanning electron microscopy (SEM), energy dispersive X-ray spectroscopy (EDX), X-ray diffraction (XRD) and atomic force microscopy (AFM). The corrosion protection of the Co and Ni samples in a marine environment (3.5% NaCl solution) was studied by the potentiodynamic polarization and electrochemical impedance spectroscopy (EIS) techniques. The results show that the addition of Im-IL inhibits Co^{2+} and Ni^{2+} deposition, which leads to more fine-grained deposits, especially at low Im-IL concentrations. The inhibition of Co^{2+} and Ni^{2+} reduction in the presence of Im-IL ions occurs *via* adsorption, which obeys the Langmuir adsorption isotherm. The CCE% is higher in the presence of Im-IL. SEM images show smoother deposits of Co and Ni in 1×10^{-5} M and 1×10^{-4} M Im-IL solution respectively. The results prove that Im-IL acts as an efficient additive for electroplating soft Co and Ni films.

Received 27th July 2020
Accepted 24th August 2020

DOI: 10.1039/d0ra06510b

rsc.li/rsc-advances

1. Introduction

Nickel (Ni) and cobalt (Co) are important engineering materials among the wide range of available electroplating materials that are commonly used in many industrial applications. The widespread use of these materials is due to their unique properties, such as excellent corrosion resistance, high heat resistance, thermal stability, high hardness value, high strength, high electrical conductivity, heat conductivity, good welding ability and good paint and formation ability.[1–5] Electrodeposited nickel is highly resistant to tarnishing, and due to its high hardness value, nickel has become an alternative to electroplated chromium in hardware, automotive, electrical and electronics applications.[6] Electrodeposited alloy films of Ni are used in the fabrication of anodes for Li-ion batteries[7] and protein microarray fabrication technologies.[8] Similarly, cobalt and its alloys are used in various magnetic and storage devices, especially in microsystem technology for the production of sensors, actuators, microrelays, inductors and magnetic devices in the computer industry.[3,4,9,10]

Investigations have studied the effects of a variety of baths, including sulfate, chloride, sulfamate, acetate, citrate, glycine and gluconate baths as well as Watts-type nickel baths, with or without additives on Ni deposits.[11–14] Moreover, cobalt deposits have been obtained from different baths containing chloride,[15] sulfate,[1] chloride and sulfate,[16] gluconate,[17] acetate[18] and citrate[19] electrolytes. However, the use of an acid sulfate bath is increasingly common due to its relatively low cost, safety features and pollution control characteristics.[20] Smoother and finer surfaces were obtained with sulfate baths than with other baths.[21]

Electrodeposited Ni and Co in the presence of some organic and inorganic additives exhibit granular, nonuniform features[22,23] with extensive microcracking on the surface,[1,12,24,25] low hardness and yield strength,[26] lack of brightness, low corrosion resistance,[27] poor cathodic current efficiency,[1,28,29] insufficient thermal stability and poor throwing power.[4,12] Some additives, such as sodium citrate and glycine, that have been used as additives in the electrodeposition of Co and Ni required high temperatures and high current densities to obtain crack-free deposits.[22,30] In addition, in some previous studies, expensive substrates, such as Au, Pt and Si, have been used.[3,9,31] In

[a]*Department of Chemistry, Faculty of Science, Universiti Teknologi Malaysia, Johor Bahru, Johor, Malaysia. E-mail: emomar@taibahu.edu.sa; madzlan@utm.my; aalfakih2011@gmail.com*

[b]*Chemistry Department, College of Science, Taibah University, Al Maddinah Al Mounwara, Saudi Arabia. E-mail: kabdalsamad@taibahu.edu.sa*

† Electronic supplementary information (ESI) available. See DOI: 10.1039/d0ra06510b

other investigations, preparing the electroplating baths was expensive because the process consumed high concentrations of metal sources and additives.[3,24,26] The use of additives in aqueous electroplating solutions is extremely important to improve the surface morphology of the deposit and crystal-building processes and to enhance the precision, durability and stability of the coating.[32,33] The importance of the additives comes from interesting effects on the growth and structure of the deposits.[34] The additives can be organic or metallic and ionic or nonionic. The additives act through adsorption on the plated surface and often are incorporated into the deposit.[35] Organic additives tend to favor the development of most crystallites with certain dominant textures, mostly inhibiting crystal growth towards other crystallographic axes.[36,37] However, some additives are noneco-friendly due to high toxicity, such as Cd^{2+} compounds[38] and thiourea,[39] as well as additional properties, such as high flammability, high volatility,[39] easy decomposition,[40] nonthermal stability and poor chemical properties.[41] Therefore, ionic liquids (ILs) have become an alternative chemical group for many existing materials for use in a variety of industrial applications, including electrochemistry and electrodeposition.[42] Ionic liquids are organic salts that are liquids at ambient temperature and are comprised of organic cations and organic/inorganic anions.[41] The most important advantage of ionic liquids is their large electrochemical windows (>5 V), which allows access to elements that cannot be electrodeposited from aqueous or organic solutions, such as Al, Mg, Ti and Ta, at moderate temperatures.[43,44] Many researchers have used ionic liquids as electroplating baths in electrodeposition processes.[34,45–50] However, a few studies have used ionic liquids as additives in electrodeposition processes.[28,41,48] Therefore, in the current work, the effect of a novel ionic liquid, namely, 1-methyl-3-(2-oxo-2-((2,4,5 trifluorophenyl)amino)ethyle)-1*H*-imidazol-3-ium iodide (Im-IL), on the coating and electrodeposition qualities of Co and Ni from sulfate and Watts baths were studied. Scanning electron microscopy (SEM), combined with energy dispersive X-ray spectroscopy (EDX), X-ray diffraction (XRD) and atomic force microscopy (AFM) were used to analyze the structures, morphologies and compositions of the coatings. For more in-depth investigation, the electrodeposition behavior and the nucleation mechanisms were investigated using cyclic voltammetry (CV) and anodic linear stripping voltammetry (ALSV). The effects of the potential scanning rate for Co and Ni deposition were determined.

2. Material and methods

2.1 Chemicals and reagents

All the chemicals and reagents were of analytical grade and were obtained from Sigma-Aldrich, Germany, and the electrolytes were freshly prepared using double-distilled water. The imidazolium iodide incorporating aromatic amide, namely, 1-methyl-3-(2-oxo-2-((2,4,5-trifluorophenyl)amino)ethyle)-1*H*-imidazol-3-ium iodide (Im-IL), M.W. = 397.15 g mol^{-1}, was synthesized through the simple quaternization of methylimidazole with fluorinated aromatic acetamide bromide in acetonitrile, Fig. 1. The newer imidazolium Im-IL ionic liquid design, synthesis steps, melting point, purity and characterization are reported in detail in ref. 51. Moreover, the newly synthesized Im-IL was fully characterized using several spectroscopic methods, such as 1H, 13C, 11B, 19F, 31P NMR, and mass analysis.[51]

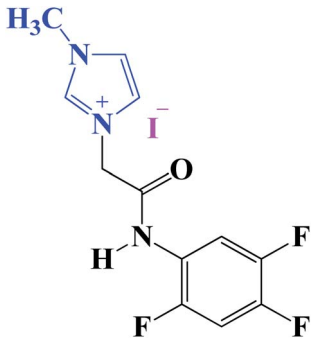

Fig. 1 The molecular structure of the ionic liquid namely 1-methyl-3-(2-oxo-2-((2,4,5 trifluorophenyl)amino)ethyle)-1*H*-imidazole-3-ium iodide (Im-IL).

2.2 Electrolyte for electrodeposition

Cobalt electrodeposition onto Cu substrates was achieved using an acidic sulfate bath containing 100 g L^{-1} of $CoSO_4 \cdot 7H_2O$, 17.02 g L^{-1} of Na_2SO_4, and 30 g L^{-1} of H_3BO_3 (ref. 1) in the absence and presence of Im-IL. The Watts bath for Ni electrodeposition onto Cu substrates contained 165.6 g L^{-1} of $NiSO_4 \cdot 6H_2O$, 21.4 g L^{-1} of $NiCl_2 \cdot 6H_2O$, and 18.6 g L^{-1} of H_3BO_3 (ref. 12 and 52) in the absence and presence of Im-IL. The pH was adjusted using 1 : 1 (H_2SO_4 : H_2O) and was measured using a pH meter (HANNA, IH 2210, ITALY).

2.3 Preparation of copper (Cu) electrode substrates and counter electrode

Copper (Cu) sheet (6.25 cm^2, 0.25 cm thick, 99.99%, Advent Research Materials) was used as the substrate. The counter electrode (CE) was a large-surface platinum sheet (6.25 cm^2, 0.25 cm thick, 99.95% metals basis, Alfa Aeser). Before each experiment, the electrodes were cleaned in pickling solution (300 ml H_2SO_4, 100 ml HNO_3, 5 ml HCl and 595 ml H_2O)[7] then dried in a desiccator.

2.4 Measurement procedures and equipment

To guarantee the accuracy of the analyses and results, the experiments were performed in duplicate using unstirred solutions, with a 10 min plating duration at a temperature of 25 °C. The electrochemical experiments were carried out in a three-electrode cell using a Gamry potentiostat/galvanostat (Gamry Interface 1000) connected to a PC and were analyzed using Gamry Echem software. Platinum and saturated calomel electrodes (SCE, HANNA, HI5412, ITALY) were used as the counter and reference electrodes, respectively. A Cu sheet or glassy carbon electrode (GCE) was used as the working electrode according to the particular technique.

2.4.1 Potentiodynamic cathodic polarization (CP) curves. Potentiodynamic cathodic polarization (CP) curves were

recorded using Cu substrates by sweeping the potential from the rest potential toward the negative direction with a scan rate of 10 mV s^{-1}.

2.4.2 Cyclic voltammetry measurements (CV). Voltammetric measurements were performed in the potential range from 1.0 to −1.5 V_{SCE}, with a scan rate of 100 mV s^{-1}. The working electrode was a GCE (a disk shaped area = 0.07 cm2, 6 mm, reorder ET 051). GCE was polished with a polishing kit using an alumina slurry (α-alumina polishing powder 0.05 mm) until a mirror surface was obtained. Then GCE was rinsed with deionized water, and sonicated in ultrasonic bath for 5 min then dry the electrode under a stream of pure nitrogen. After electrodeposition, the produced coatings were rinsed by deionized water and ultrasonically treated to remove the deposits from the surface.

2.4.3 Situ-anodic linear stripping voltammetry (ALSV) measurements. For situ-anodic linear stripping voltammetry measurements, Co or Ni deposition was carried out at a constant potential (−1.0 V_{SCE}) on the GCE for a constant plating time (100 s) at 25 °C. Potentiodynamic polarization resistance (PPR) analysis and chemical composition analysis were performed immediately after potentiostatic deposition from the potential (−0.4 V) toward more anodic potentials (0.5 V) at a scan rate of 10 mV s^{-1} (ref. 1, 12 and 52) without removing the working electrode from the solution.

2.4.4 Cathodic current efficiency (CCE%). A direct current was supplied using a DC power supply unit (QJ3005A, ITALY) to measure the CCE% of the Co and Ni electrodepositions at different current densities, times, pH and potentials without and with different concentrations of Im-IL. A Cu sheet cathode and Pt sheet anode (6.25 cm^2) were used to generate a composite coating. The CCE% is calculated from eqn (1)[1]

$$\mathrm{CCE\%} = \frac{W_p}{W_t} \times 100 \quad (1)$$

where W_p is the practical weight of the deposit, and W_t is the theoretical weight of the deposit calculated using Faraday's law.

2.4.5 Characterization techniques. The surface morphology of the Co- and Ni-coated samples was examined using a scanning electron microscope (SEM, JEOL JSM-6000, Shimadzu, Japan) equipped with energy dispersive X-ray spectroscopy (EDX) microanalysis hardware using an accelerative voltage of 15 kV. The phase and crystal structure of the Co and Ni films were analyzed by X-ray diffraction (XRD, Shimadzu, XRD-7000, Japan) using monochromatic Cu Kα radiation (k = 1.5406 Å) operated at 40 kV and 30 mA with a 2θ angle pattern. To provide superior topographic images, atomic force microscopy (AFM, digital instrument CP-II, Veeco Company, USA) measurements were carried out in contact mode.

2.4.6 Corrosion resistance measurements. The corrosion protection performance of the Co and Ni samples in a marine environment (3.5% NaCl solution) was studied by the potentiodynamic polarization and electrochemical impedance spectroscopy (EIS) techniques. These electrochemical experiments were carried out at 25 °C using a classic three-electrode cell with a platinum sheet as the counter electrode and a saturated calomel electrode (SCE) as the reference. The electrodeposited Co or Ni samples were used as the working electrode. Before the corrosion experiments, the samples were first immersed into the 3.5% NaCl solution for approximately 30 min to stabilize the open-circuit potentials (OCPs). The EIS measurements were carried out in the frequency range between 100 kHz and 0.01 Hz with an amplitude of 10 mV with a superimposed AC signal, and the corresponding Nyquist plot was obtained. Then, potentiodynamic curves were recorded by scanning with a scan range of ±700 mV and a scan rate of 1 mV s^{-1} with respect to OCP.

2.4.7 Microhardness measurements. Microhardness measurements were performed on some Co or Ni as-plated samples. The time of plating was 60 min to obtain thick deposits. In all the tests, 25 grams-force load was employed, and the indentations were made directly on the plated surface parallel to the base metal. The microhardness of the electrodeposited coatings is usually determined using a conventional microhardness technique in which a Vickers indenter is used (Model Hysitron TI 725 Ubi., USA). The average of five readings was taken along the circumference of a circle as a measure of the microhardness of each sample. The results are expressed as Vickers hardness number (VHN).

3. Results and discussion

3.1 Cathodic polarization (CP)

Cathodic polarization (CP) curves are important for understanding the nature of electrodeposition. This method is considered a useful technique for characterizing the influence of additives on the electrodeposition process. To improve the nature of the Co and Ni deposits, Im-IL was added to the bath solutions. The effects of Im-IL on the cathodic polarization curves of the Co and Ni electrodeposits at pH 4.5 (ref. 1) are shown in Fig. 2a and b. The cathodic branch curves were swept from the rest potential of approximately −0.3 V_{SCE} to −1.6 V_{SCE}. In free solution, a high polarization accompanies the deposition of Co and Ni from aqueous solutions. Im-IL causes a slight shift toward more a negative overpotential in the polarization curves of Co electrodeposition, whereas the effect of Im-IL is more pronounced for nickel electrodeposition. A high polarization shift toward a more negative overpotential and a significant decrease in the cathodic current was observed. The cathodic polarization potential (CPP) of Co and Ni electrodeposition in free solution was approximately −0.83 V_{SCE} and −0.97 V_{SCE}, respectively, at 2.0 × 10^{-3} mA cm^{-2}. The simultaneous discharge of hydrogen ions was observed during the deposition of the Co^{2+} and Ni^{2+} ions. As the Im-IL concentration increased from 1 × 10^{-6} M to 1 × 10^{-3} M (Fig. 2a and b), the cathodic polarization potential of both metals became increasingly negative, T1. The higher inhibition effect of Im-IL on Ni electrodeposition was confirmed from the high CPP value. The presence of Im-IL increased the polarization of the cathode toward a more negative overpotential, *i.e.*, it decreased the current density obtained for a given electrode potential. The influence of Im-IL on hydrogen liberation may be explained according to the hydrogen release mechanism. This mechanism is shown in the following eqn.[53]

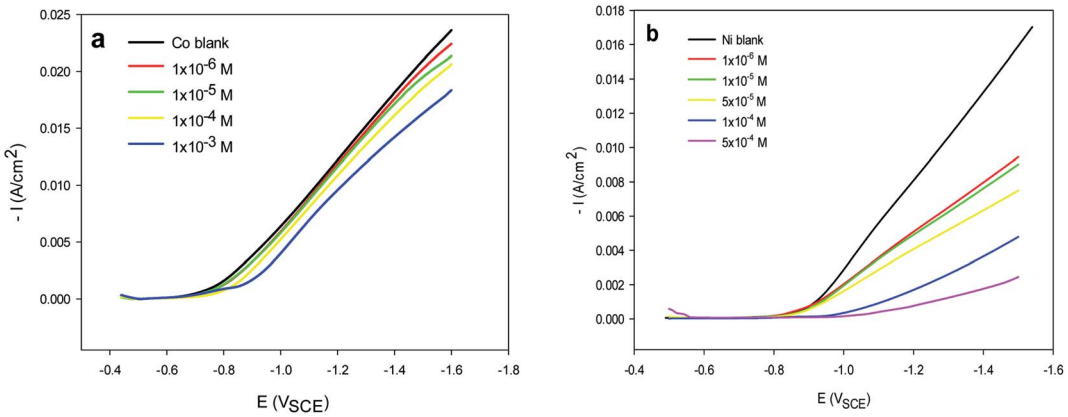

Fig. 2 Potentiodynamic cathodic polarization (CP) curves for (a) Co and (b) Ni electrodeposition in the absence (blank) and presence of different concentrations of Im-IL at pH 4.5.

$$H^+ + e \rightarrow H_{ads} \quad (2)$$

$$2H_{ads} \rightarrow H_2 \quad (3)$$

Im-IL is supposed to block the association of the electrolytically generated hydrogen atoms, eqn (2), allowing the concentration of H_{ads} to decrease and thus decreasing the rate of hydrogen evolution, eqn (3). The inhibitory effect of Im-IL could be attributed to its adsorption on the metal surface.[40] The mechanism for Im-IL adsorption on the surface of the metal electrodes can be explained based on the Im-IL structure. As shown in Fig. 1, the Im-IL molecule contains a positive charge on the quaternary nitrogen atom of the imidazole ring. When electrical current is applied to the working electrode, the positively charged Im-IL is reduced on the surface of the electrode and is then adsorbed to energetically favorable surfaces of the metal electrode (low energy surfaces), thus leaving only the high energy surfaces available for metal deposition.[37] This process creates a network of the cationic ionic liquid on the electrode surface and hinders the formation of large Co and Ni crystals.

The explanation of imidazole derivatives Im-IL ionic liquids as additives performance during electrodeposition of Ni and Co based on its molecular structure properties as shown in Fig. 1. The inhibiting effect of the studied Im-IL can be attributed to its parallel adsorption on the Cu substrate surface. The parallel adsorption of this molecules is attributed to the presence of more than one active center for adsorption. These active centers in the Im-IL chemical structures, Fig. 1, are as the following:

- Imidazole ring consists of two nitrogen atoms as heteroatom that have lone pair of electrons and 4 π-electrons of two conjugated double bonds in the imidazole ring in the chemical structures of Im-IL.

- Six π-electrons of three conjugated double bonds in phenyl ring of ionic liquid Im-IL.

- Amid function group in Im-IL which have two π-electrons of one double bond as well as nitrogen and oxygen heteroatoms with one and two lone pair electrons, respectively.

- Three fluorine atoms as heteroatoms contain nine lone pair electrons on phenyl group in Im-IL.

In general, as the number of double bond increase, π-electrons increase and adsorption on the cathode surface becomes easier.[33] As Ni and Co plating ionic liquid additives, Im-IL with 6 π-electrons can be better adsorbed on the cathode surface and consequently increase the polarization of the Ni and Co electroplating the most. Moreover, oxygen atoms have the property of electron donation, which is associated with its strong adsorption ability on the metal surface.[54] Nitrogen atoms among the nitrogen heterocyclic compounds were preferred active sites for accepting electrons from Cu substrate.[55]

The inhibitory effect of the Im-IL molecule can also be attributed to the specific adsorption of iodide ions on the cathode surface, as reported in ref. 40. Iodide anion adsorption leads to an increased density of the negative charges on the substrate surface, which results in an increase in the attraction of Im-IL cations. It can be concluded that the adsorption processes increase the overpotential by decreasing the sites available for the discharge of Co^{2+} and Ni^{2+} ions.[40]

3.1.1 Tafel lines and electrode kinetics. Measurements of cathodic polarization curves under carefully controlled conditions can yield information about coatings, films, passivity and kinetics. In an acidic medium, hydrogen gas evolves at the cathode, which always competes with the Co^{2+} and Ni^{2+} reduction process. Important information regarding the mechanism of hydrogen reduction in the presence of additives can be obtained from the current–potential relationship, Fig. 2. Table 1 summarizes the kinetics data (η, overpotential (V); a, constate; b_c, cathodic Tafel slope (mV dec^{-1}); i_c, cathodic current density (A cm^{-2})) extract by applying the Tafel equation.

$$\eta_c = a + b_c \log i_c \quad (4)$$

The transfer coefficient (α_c) can be determined from eqn (5).

$$b = RT/\alpha nF \quad (5)$$

Table 1 Tafel kinetic parameters obtained for Co and Ni deposits in the absence and presence of different concentrations of Im-IL

Co				Ni			
[Im-IL] (M)	b_c (mV per decade)	i_o (A cm^{-2})	α_c	[Im-IL] (M)	b_c (mV per decade)	i_o (A cm^{-2})	α_c
0	−347	1.90×10^{-3}	0.0371	0	−266.0	3.16×10^{-3}	0.0482
1×10^{-6}	−271	3.91×10^{-3}	0.0474	1×10^{-6}	−253.4	2.85×10^{-3}	0.0507
1×10^{-5}	−268	4.08×10^{-3}	0.0479	1×10^{-5}	−253.6	2.79×10^{-3}	0.0506
1×10^{-4}	−246	4.87×10^{-3}	0.0521	5×10^{-5}	−253.7	2.50×10^{-3}	0.0506
1×10^{-3}	−202	7.32×10^{-3}	0.0636	1×10^{-4}	−147.0	7.17×10^{-3}	0.0873
—	—	—	—	5×10^{-4}	−141.0	6.05×10^{-3}	0.0909

where n is the number of electrons and R and F are always the gas constant and Faraday's constant, respectively.[56] The slight change in b_c in either the absence or presence of Im-IL in Table 1 confirms that there is no change in the mechanism of the reduction process. Moreover, Table 1 shows that as the Im-IL concentration increases, the cathodic current density, i_c, is notably decreased. In general, the current density decreases when the electrochemical reaction is inhibited.[1,40] This finding implies that Im-IL decreases and inhibits the rate of Co^{2+} and Ni^{2+} transfer across the electrical double layer. The inhibitory effect of Im-IL could be due to its adsorption to energetically favorable sites of the metal electrode (low energy surfaces), thus leaving only the high energy surfaces available for metal deposition on the metal surface.[37] The presence of an adsorbate alters the double-layer structure and decreases the rate of the electrochemical reaction.[40,52,57] The increase in the values of the transfer coefficient, α_c, in the presence of Im-IL implies that the charge transfer reaction is affected by the presence of Im-IL[1] and is associated with differences in the morphological characteristics of the deposits.[40] The increase in the i_c for the Ni^{2+} electrodeposition at low Im-IL concentrations could be attributed to the induction of hydrogen evolution due to the adsorbed Im-IL ions on the Cu substrate and Ni deposit at high energy sits and lower the hydrogen overpotential. Similar observations were obtained during Zn electrodeposition in the presence of copper as an impurity from an acidic sulfate electrolyte.[57]

3.2 Adsorption isotherms

Adsorption isotherms provide information regarding the interaction between the Im-IL additive and metal deposited films. The adsorption of Im-IL molecules at cathodic sites increases the overpotential by decreasing the sites that are available for the discharge of Co^{2+} and Ni^{2+}. The experimental data from potentiodynamic cathodic polarization curves were used for the adsorption isotherm study. The surface coverage (θ) can be estimated from eqn (6).[40]

$$\theta = (1 - i_{add}/i) \quad (6)$$

where i and i_{add} are the current density in the absence and presence of the additive, respectively, at a constant potential (−1.4 V_{SCE}) for Co and Ni. According to the data in T1, the θ values increase with the increasing concentration of Im-IL as both ions deposit. The surface coverage is high for Ni^{2+} reduction, which indicates a greater adsorption rate of Im-IL ion on the cathode surface.

The data are fitted by the Langmuir adsorption isotherm, eqn (7).[40]

$$\theta/1 - \theta = K[C] \quad (7)$$

where K is the equilibrium constant of the adsorption reaction, and C is the Im-IL concentration in the bulk of the solution. From S1,† the calculated K value is 229.5 M^{-1} and 11 625.8 M^{-1} for Im-IL adsorption for the Co^{2+} and Ni^{2+} baths, respectively. The larger value of K indicates higher adsorption of a given compound, *i.e.*, stronger electrical interactions between the double layer existing at the phase boundary and the adsorbing molecules. The adsorption constant, K, is related to the standard free energy of adsorption (ΔG_a°) based on eqn (8).[58]

$$\Delta G_a^\circ = -RT \ln(55.5\,K) \quad (8)$$

where R is the gas constant, T is the absolute temperature and the value 55.5 is the molarity of water. The negative value of ΔG_a° indicates a spontaneous process for the adsorption of Im-IL molecules on the copper surface. In general, values of ΔG_a° as great as −20 kJ mol^{-1} are compatible with physical adsorption *via* electrostatic interaction between the charged molecules and charged metal, whereas values that are more negative than −40 kJ mol^{-1} are consistent with chemical adsorption *via* the sharing or transfer of electrons from inhibitor molecules to the metal surface to form a coordination bond.[58] The calculated ΔG_a° values of Im-IL in the presence Co^{2+} and Ni^{2+} are equal to −23.4 and −33.1 kJ mol^{-1}, respectively, which fall between these two values for physical and chemical adsorption. This result indicates that the adsorption of Im-IL onto the copper substrate surface during the Co and Ni electrodeposition process involves both chemical and physical adsorption (a mixed type) mechanisms.[59] However, the higher value of ΔG_a° in the presence of Ni indicates that this metal experiences higher adsorption on the copper substrate surface. These results agree well with the high overpotential in the cathodic polarization curves of Ni electrodeposition in the presence of Im-IL. Similar results were reported for other ionic liquid molecules.[40,60] The results also show that the inhibition of Co and Ni deposition could be due to the specific adsorption of iodide ions on the Cu

substrate surface, which creates an excess negative charge toward the solution and favors the increased adsorption of Im-IL cations. In short, the adsorption of Im-IL cations between the metal and solution interface is usually accepted as the formation of electrostatic or covalent bonding between the adsorbate and the metal surface atoms. In other words, halide ions adsorb on the metal surface by creating oriented dipoles with their negative ends toward the solution, thus increasing the adsorption of the Im-IL cations on the dipoles.

3.3 Cyclic voltammetric behavior of the deposition process

Cyclic voltammetry (CV) was used to define the reduction potential regions and to provide qualitative information and characterization of the metal deposition processes under various conditions, such as the presence of intermediates in oxidation–reduction reactions.[56] The cyclic voltammetry measurements were carried out on a GCE for the electrodeposition of Co^{2+} and Ni^{2+} from acidic media baths over a potential range of 1.0 to −1.5 V_{SCE} with a scan rate of 100 mV s^{-1} in the absence and presence of Im-IL (Fig. 3a and b). In the negative direction, the cathodic current commences at approximately −0.9 associated with the onset of Co and Ni nucleation at point A and reduction in the sulfate and Watts baths, respectively. The current increases sharply when the scan proceeds toward more negative potentials (>−1.0 V_{SCE}), corresponding to Ni and Co depositions with metallic light gray deposits and the coevolution of H_2. The coevolution of H_2 becomes visible with the formation of H_2 gas bubbles at the edges of the deposited layer on the WE beyond −1.4 V_{SCE}. The current then increases to its highest value at point B. On reverse scan, the current decreases and consequently reaches zero current at the crossover potential (−0.5 V_{SCE}), point C. The current then becomes anodic, corresponding to the dissolution of the cathodically deposited Co, point D, as shown in Fig. 3a. No oxidation current was observed in the anodic scan, Fig. 3b, indicating that the Ni electrodeposit cannot be dissolved in the bath. This observation proves that Ni deposits strongly adhere copper.[12,18,32,61] The presence of Im-IL in the range of 1×10^{-6} to 1×10^{-3} M shifts the deposition overpotential to more negative values and inhibits Co^{+2} and Ni^{+2} deposition, as illustrated in Fig. 3a and b. This behavior is due to the adsorption of Im-IL on the low-energy active sites, leaving the high-energy sites for metal depositions, as confirmed in the results of the cathodic polarization curves. A similar additive behavior was reported for Ni[62,63] and Zn electrodeposition.[40,60]

In the electrodeposition process, the CV technique is considered mainly to determine the formal reduction and nucleation overpotential (NOP).[40] NOP is used to explain the extent of polarization of a cathode. From the nucleation overpotential, it can be observed that an additional potential is necessary before starting the first reduction. The potential difference between the reduction potential at point A and the crossover potential at point C is a measure of NOP. The high NOP values in T2 indicate strong polarization.[56] This observation supports the other obtained results, *i.e.*, no anodic peak in CV, high value of K, ΔG° and substantial shift to a more negative potential in the cathodic polarization curves, especially in the case of Ni.

The effect of the scan rate on the electrodeposition behavior of Co and Ni in the presence of 1×10^{-5} M Im-IL is displayed in S2a and b.† As expected, the increase in the scan rate shifts the Co and Ni reduction peaks to more negative potentials and produces a higher current contribution. This result explains why the electrodeposition behavior is qualitatively affected by the scan rate. A current crossover also occurs in the cathodic branches when the nucleation overpotential increases with the scan rate, indicating a typical nucleation process for deposition. For a diffusion-controlled system, the Randles–Sevcik equation best describes the electrochemical behavior of an irreversible process. For an irreversible process, the cathodic peak current (i_{pc}) is proportional to the square root of the scan rate ($v^{1/2}$), eqn (9):[64]

$$i_{pc} = (2.99 \times 10^5) D^{1/2} \alpha^{1/2} C A n^{3/2} v^{1/2} \quad (9)$$

where D is the diffusion coefficient ($cm^2\ s^{-1}$), α is the electron transfer coefficient, C is the concentration in mol dm^{-3}, A is the electrode area (cm^2), and n is the number of electrons transferred in the redox event. The linear relation between i_{cp} and $v^{1/}$

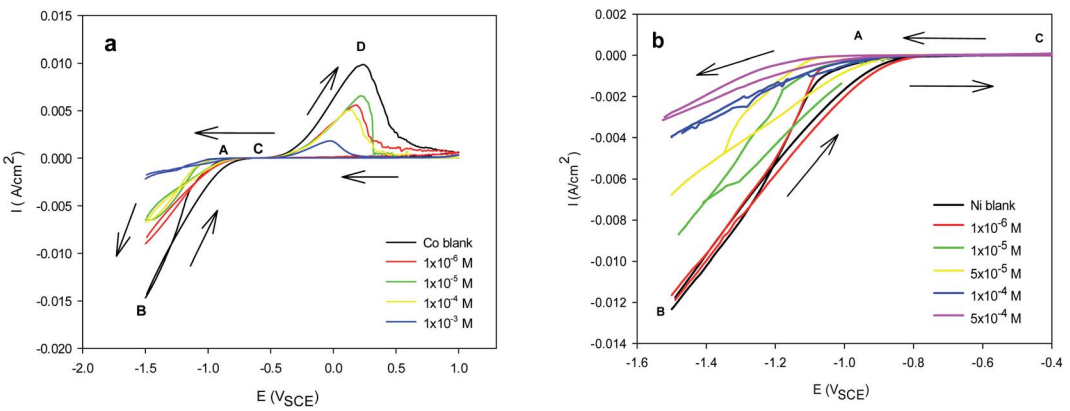

Fig. 3 CVs for (a) Co and (b) Ni electrodepositions recorded at GCE in the absence and presence of different concentrations of Im-IL at scan rate 100 mV s^{-1}.

^{2}, S2a and b,† suggests that the rate of growth is controlled by the mass transfer of Co^{2+} and Ni^{2+} to the growing center. Similar electrochemical results have recently been reported for Co^{2+} in a reverse micellar solution,[64] for Zn in an acidic bath in the presence of ninhydrin as an organic additive,[40] in 1-butyl-3-methylpyridinium bromide [BMPy] Br ionic liquid additive[60] and for brass alloy in an ammonia bath.[65]

3.4 *In situ*-anodic linear stripping voltammetry (ALSV)

Anodic stripping voltammetry is a voltammetry method for the quantitative determination of specific ionic species. This method is particularly useful as a simple and easy '*in situ*' electrochemical method for identifying the phase and composition of metals and alloys. The analyte of interest is electroplated on the working electrode during a deposition step and oxidized from the electrode during a stripping step. The current is measured during the stripping step. The oxidation of the species is registered as a peak in the current signal at the potential at which the species begins to be oxidized.[66] After the plating of Co^{2+} and Ni^{2+} on the GCE at -1.0 V_{SCE} for 100 s, the potential was immediately swept linearly in the positive direction at a scan rate of 10 mV s^{-1}, and an anodic stripping voltammogram was recorded without removing the electrode from the solution. As shown in Fig. 4a and b, the voltammograms have only one oxidation peak, which results from the oxidation of only the Co or Ni that was previously potentiostatically deposited on the GCE. Visual observation of the GCE after reaching the anodic peak did not show any residual Ni or Co. Therefore, the charge used for anodic stripping can be taken as an estimation of the current efficiency of the Co or Ni deposition process, *i.e.*, the area under the peak is equivalent to the amount of Co or Ni deposited. From Fig. 4 and T2, it is clear that both the stripping current and the area under the stripping peak have been greatly suppressed in the presence of Im-IL for both Co and Ni. This result indicates that Im-IL acts as an inhibitor for Co^{2+} and Ni^{2+} deposition. The inhibition process increases with increasing Im-IL concentration. These results agree well with the data of the polarization curves in Fig. 2. However, it is obvious that the electrical charge consumed with the potential of the anodic peak of Ni is very small when compared with that of Co, confirming the small amount of Ni deposited on the GCE.[17] The easier oxidation of the Co deposited in the presence of Im-IL led the potential shift to the less noble direction.[14] The opposite behavior of the stripping potential for the Ni deposited in the presence of Im-IL was due to the difficulty of Ni dissolution.[12]

3.5 Cathodic current efficiency

The current efficiency is the ratio of the actual mass of a substance liberated from an electrolyte by the passage of

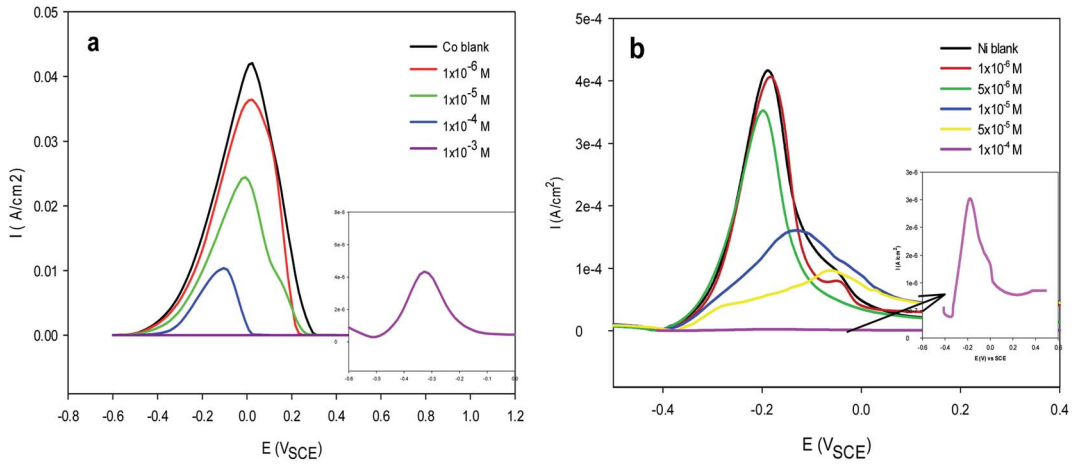

Fig. 4 ALSVs for (a) Co and (b) Ni electrodeposition in absence and presence of different concentrations of Im-IL.

Table 2 The operating and best conditions of Co and Ni electrodepositions which used at CCE% studies

		Best conditions	
Operating conditions	Range	Co	Ni
Current density/mA cm^{-2}	6–24	20	20
pH	3.5–4.5	4.5	4.5
Deposit potential/V	3–9	6.5	6.6
Deposit time/mint	3–15	10	10
[Im-IL]/M	From 1×10^{-6} to 1×10^{-3}	1×10^{-5} 1×10^{-4}	5×10^{-5} 1×10^{-4}

current to the theoretical mass liberated according to Faraday's law. The cathodic current efficiency, CCE%, was calculated during metal electrodeposition at different operating conditions, including current density, pH, plating time and deposit potential, in the absence of Im-IL to determine the optimal bath conditions. The operating conditions and best conditions for Co^{2+} and Ni^{2+} electrodeposition are given in Table 2. At the optimal conditions, the CCE% value was nearly 100%. T3 presents the CCE% values of Co and Ni electrodeposition with different Im-IL concentrations. Interestingly, a slight improvement in the CCE% values in the preferred Im-IL concentration, Table 2, supported the effective role of Im-IL in the Co and Ni electrodepositions in contrast to glycine, which decreased the CCE% during Co and Ni electrodepositions, as reported in ref. 1 and 12. In general, most additives have no significant effect on the CCE% of metal deposition. However, additives did affect the surface morphology and crystallographic orientation.

At the optimal bath conditions, visual observation of the Co coatings deposited from acidic sulfate baths showed that the deposit had lustrous appearance with a light gray color in the presence of Im-IL, T3, compared to the pale and hollow gray deposit obtained in the absence of Im-IL. Moreover, a very bright silver Ni deposit was obtained in the presence of Im-IL, T3. It can be concluded that the electrolytes in this work can be used to obtain bright Co and Ni deposits without the addition of brightening agents such as saccharine, sodium saccharin and boric acid. For instance, in contrast to this present work, other studies used brightening agents in the electrodeposition of Co and Ni from a hydrophobic room-temperature ionic liquid, 1-butyl-1-methylpyrrolidiniumbis (trifluoromethyl sulfonyl) amide (BMPTFSA)[25] and acidic sulfate bath.[3]

3.6 Crystal structure and surface morphology

The surface morphology in Fig. 5 and 6 was determined using SEM imaging of the Co and Ni deposits from the aqueous acidic sulfate and Watts baths, respectively. The test conditions were 20 mA cm^{-2}, pH 4.5, 20 °C and $t = 10$ min in the absence and presence of Im-IL. The Cu substrate has a flat and smooth surface in Fig. 5a and a′. In the Im-IL-free bath, the Cu substrate is almost covered by granular, nodular and large spherical grains of Co deposited (grain size of 1.08 μm) with some dimples, as can clearly be seen in Fig. 5b and b′, whereas the mud-like structure of larger grains sizes can be seen for the Ni deposit in Fig. 6a and a′ (grain size of 1.457 μm). This surface was unfavorable for deposits due to the coevolution of H_2, as clarified in the cathodic polarization curves and CV measurements. The presence of appropriate Im-IL concentrations in the electrolyte (1×10^{-5} M and 1×10^{-4} M in the Co and Ni baths,

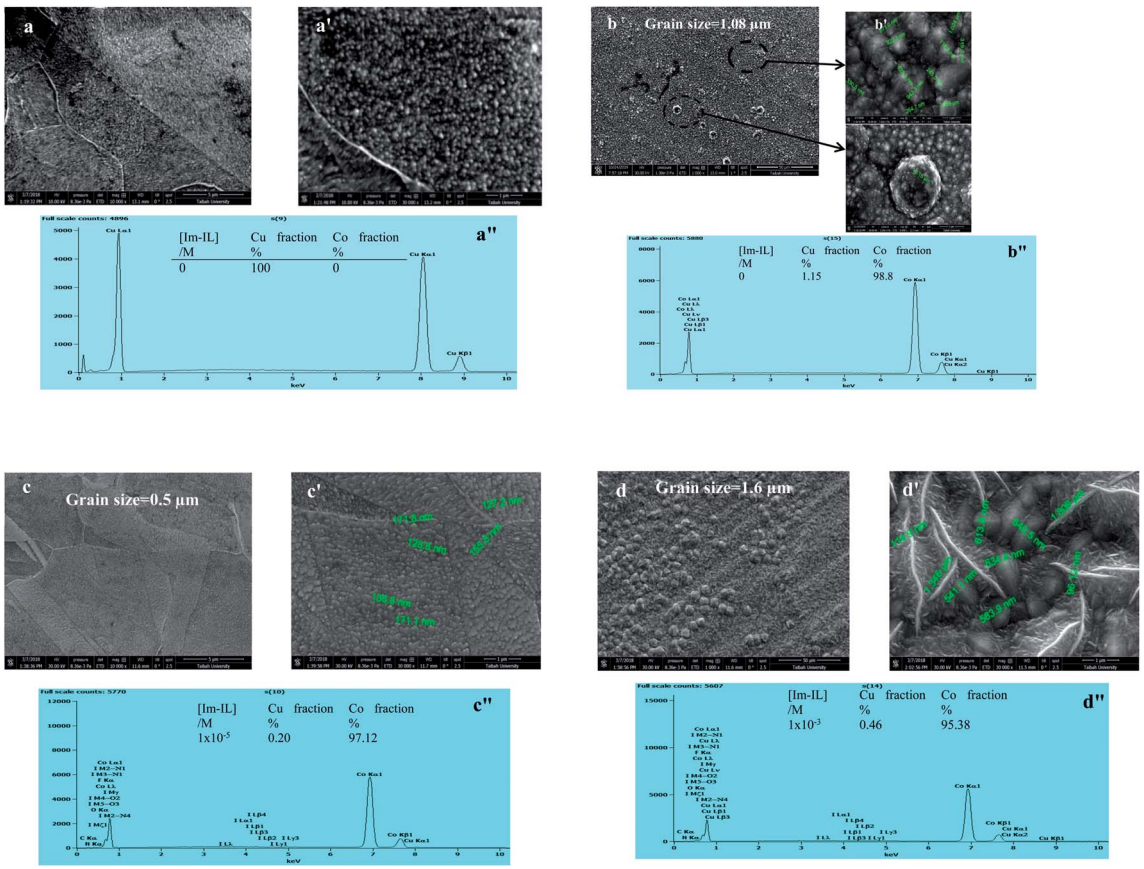

Fig. 5 SEM images, high magnification SEM and EDX spectra of (a, a′ and a″) Cu substrate, Co deposited from bath (b, b′ and b″) free Im-IL, (c, c′ and c″) 1×10^{-5} M Im-IL, (d, d′ and d″) 1×10^{-3} M Im-IL.

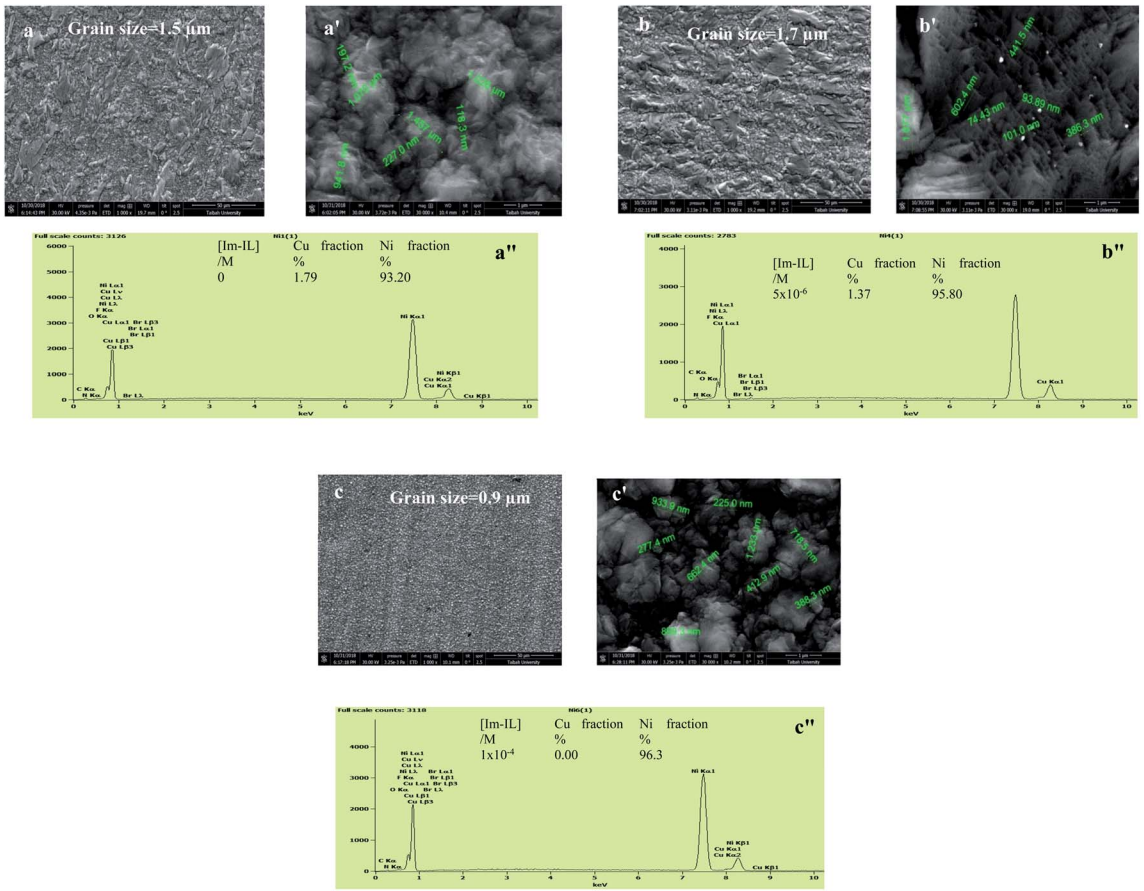

Fig. 6 SEM images, high magnification SEM and EDX spectra of Ni deposited from bath (a, a′ and a″) free Im-IL, (b, b′ and b″) 1×10^{-4} M Im-IL, (c, c′ and c″)5×10^{-6} M Im-IL.

respectively) favored the formation of compact, smoother, more leveled and brighter Co, Fig. 5c and c′, with a grain size of 0.5 μm, and of Ni, Fig. 6b and b′, with a grain size of 0.93 μm, which formed a layer with finer, less granular and more ordinated crystals that were homogeneously distributed on the surface of the cathode. The enhancement in the morphology of the metal deposits can be explained based on the effective role of Im-IL during the electrodeposition processes. Co and Ni electrodeposition processes are associated with growth and nucleation processes. The addition of Im-IL restricts the growth of Co and Ni nuclei, favoring nucleation events. This is due to the adsorption of Im-IL on the energetically favorable surfaces (the low-energy surfaces), which leads to significant hindrance for H_2 evolution as the H_2 evolution process causes pitting and cracks in the deposits surface. Thus, the adsorption of Im-IL leaves only the high-energy surfaces available for metal deposition.[37] Interestingly, microcrack-free Co and Ni deposits were obtained in current work. In previous studies, cracked Co films were obtained by adding coumarin and thiourea[2,67] as organic additives and sodium gluconate[4] and glycine[1] as complex agents in similar conditions. Likewise, cracked Ni deposits were obtained with a combination of vanillin, sodium lauryl sulfate and gelatin in Re–Ni alloys from aqueous solutions[68] and facile from alkaline media.[69] However, at a higher Im-IL concentration (1×10^{-3} M), the grain shape changes completely from spherical to a larger elliptical shape (grain size of 1.6 μm) and many creaks appear at the surface of the Co deposit, as shown in Fig. 5d and d′. Furthermore, at a lower Im-IL concentration (5×10^{-6} M), a darker layer of Ni with a scaly appearance (grain size of 1.677 μm) characterized by submicron pores and pits appeared (Fig. 6c and c′). This phenomenon appeared due to the increase in H_2 evolution as a result of the higher overpotential, which is not favorable for deposit quality. In general, the cracks and pits were probably caused by the increased overpotential and the consequent internal stress produced.[25]

Typical EDX patterns of the Cu substrate and Co and Ni coatings deposited from the various Im-IL concentrations are displayed in Fig. 5a″–d″ and 6a″–c″, respectively. As it can be seen, the Cu fractions before electrodeposition processes were 100%, indicating a pure substrate, Fig. 5a″. After coating, the substrate surface was nearly completely covered with Co deposit (98.80%), whereas slightly less was covered with the Ni deposit (93.20%). The addition of Im-IL at different concentrations decreased the Co fraction and increased Ni fraction, as shown in Fig. 5c″, d″, 6b″ and c″. As the Im-IL concentration was increased, the Co fraction decreased while the fraction of other elements increased due to the adsorption of Im-IL on the Cu

surface. Even so, Im-IL enhanced the surface coverage of the Ni deposits.

To provide more surface structural details of the formed electrodeposited films, AFM was used. Three dimensional (3D) and two dimensional (2D) topographical images and roughness parameters of the Cu substrate and Co and Ni deposits in the absence and presence of Im-IL are depicted in S3 and S4.† The morphology of the Cu substrate as recorded in 3D nuclei imaging was found to be a flat surface. As shown in S3(a and a′),† the average roughness, R_a, and the total roughness, R_t, values were 13 nm and 16.46 nm, respectively. The high roughness of the Im-IL-free deposits, S3b, b′, S4a and a′,† is evidenced by greater variation between the peaks and valleys of the topography, with $R_a = 0.137$ μm, $R_t = 0.178$ μm in the Co film and $R_a = 66.9$ nm and $R_t = 86.9$ nm in the Ni film. This variation is due to irregular growth and the random distribution of grains during electrodeposition due to the degree of high polarization and coevolution of H_2, as documented by SEM. In contrast, the coatings showed the lowest roughness, with $R_a =$ 59.6 nm, $R_t = 74.3$ nm in the Co film when in the presence of 1×10^{-5} M Im-IL and $R_a = 36.7$ nm and $R_t = 45.1$ nm in the Ni film when in the presence of 1×10^{-4} M Im-IL (S3c, c′, S4b and b′†). The least roughness and lowest nucleation rate of the grains during electrodeposition allowed for good lateral growth, making the coating more compact and uniform than in the Im-IL-free coating. This result occurs due to the adsorption of Im-IL on the energetically favorable surfaces and the fact that H_2 evolution was significantly blocked. S3d, d′, S4c and c′† show the surfaces with the greatest roughnesses, obtained at 1×10^{-3} M for Co and 5×10^{-6} M for Ni, with variation between the peaks and valleys measured to give $R_a = 83.6$ nm, $R_t =$ 104.99 nm in the Co film and $R_a = 66.15$ nm, $R_t = 83.8$ nm in the Ni film. This appearance can be explained by the low cathodic current densities in the presence of Im-IL in the CV measurements of both Co and Ni during electrodeposition, which contributed to an increase in the activation overpotential of both H_2 evolution and Co and Ni reductions.[32] This result is also in good agreement with the obtained findings by visual observation from the SEM analysis. Similar behaviors were obtained for saccharin as an additive[3] and glycine as a complexing agent[7] in other Co and Ni electrodeposition experiments.

The XRD patterns in Fig. 7 agree well with the face-centered cubic (FCC) Cu substrate (JCPDS 00-004-0836), Co (JCPDS 00-015-0806) and Ni (JCPDS 00-004-0850) in the absence and presence of 1×10^{-5} M of Im-IL in the Co and Ni baths. The same FCC pattern with a strong (2 2 0) diffraction peak in Fig. 7 is present at nearly $2\theta = 75.8°$. THus, most of the Co and Ni crystallites are oriented parallel to the (2 2 0) plane. It is worth mentioning that although Im-IL significantly affects crystallographic orientation (texture) in the metals deposited only, (no chemical change occurs), no shifts occur in the diffraction peaks relative changes in the peak brightness. The average crystal sizes of the FCC (2 2 0) calculated using the Scherrer equation for the Ni and Co films electrodeposited in the presence of Im-IL were 21.55 nm and 20.70 nm respectively, which are smaller than the FCC (2 2 0) crystal size of both metal films deposited from the Im-IL-free baths (30.86 nm for Ni and 23.46 nm for Co). This result indicates that Im-IL is more affective in improving the surface morphology of Ni deposits than Co deposits. It has been reported that the inclusion of multiwalled carbon nanotubes (MWCNTs),[70] nicotinic acid (NA), boric acid (BA) and benzoquinone (BQ),[34] ionic liquid 1-butyl-3-methylpyridinium bromide,[60] 2,2-bipyridine[71] and sodium thiosulfate[72] as additives on the metal matrix can modify the grain orientation.

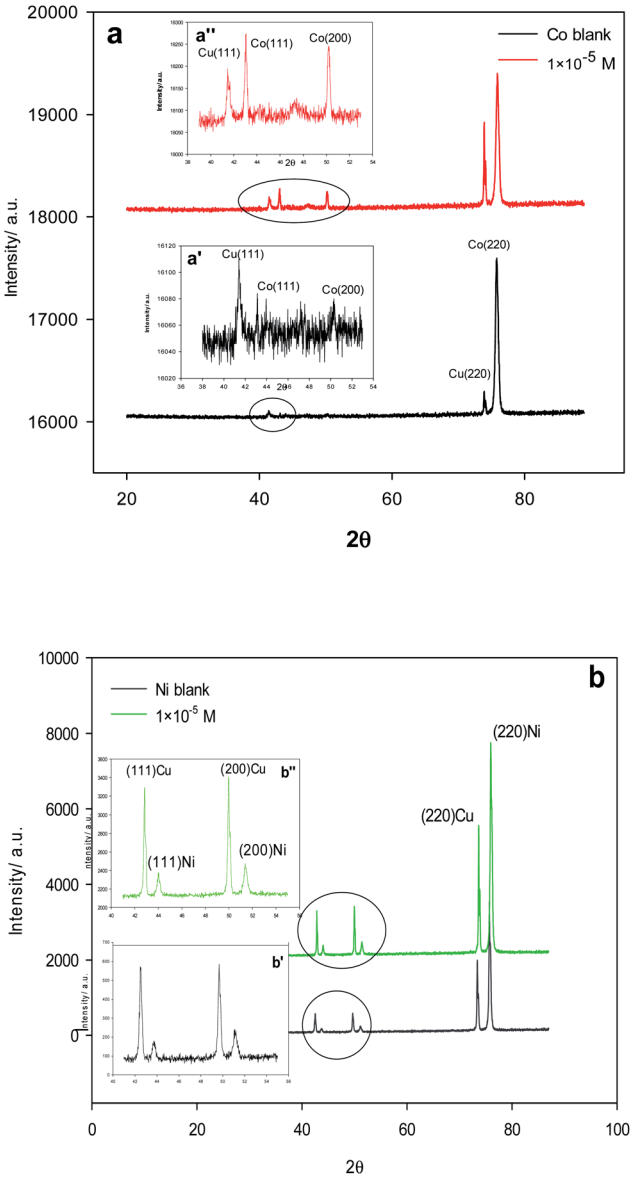

Fig. 7 XRD patterns of Cu substrate, (a, a′ and a″) Co deposits, (b, b′ and b″) Ni deposits in absence and presence of 1×10^{-5} M Im-IL.

The Vickers microhardness Hv (kg f mm^{-2}) for the Co and Ni deposited from the Im-IL and Im-IL-free baths was measured. The data in T4 reveal hardness values of approximately 368.5 Hv and 270 Hv for Co and Ni, respectively, in the 1×10^{-5} M Im-IL bath compared to 342.5 Hv and 211.25 Hv for Co and Ni, respectively, from the Im-IL-free bath. According to the data above, the hardness of Co deposits is greater than that of Ni

deposits in the absence and presence of Im-IL, and Im-IL efficiently improves the hardness of both the Co and Ni films. Interestingly, the microhardness of the Co deposits from the Im-IL baths is greater than that of the Co deposits in the presence of gluconate (341 Hv)[4] or sodium dodecyl sulfate (SDS) (343 Hv)[70] and Ni deposits in the presence of Natural Kermes Dye (NKD) (225 Hv)[52] from acidic baths.

The ongoing interfacial reactions and characteristics of the coating corrosion properties were detected using EIS measurements. The measurements were conducted for Co and Ni deposits in the absence and presence of Im-IL in the frequency range from 100 kHz to 0.01 Hz. The Nyquist plots for Cu and the Co and Ni films in 3.5% NaCl in the absence and presence of 1×10^{-5} M Im-IL are shown in S5a and b, while S5c and d† shows the compatible equivalent circuit for the Nyquist plots with the parameters for the impedance spectra. The solution resistance (R_s), charge transfer resistance (R_{ct}), constant phase element (CPE), degree of roughness (n) and the Warburg impedance (W) parameters are listed in T4, with a χ^2 of approximately 1×10^{-3} to 1×10^{-6}. From S5a,† for the Co deposit, the plots show one depressed capacitive loop, which is often attributed to frequency dispersion resulting from inhomogeneity or surface roughness.[58,73] The Im-IL significantly affects the high- and low-frequency loop. The diameters of the capacitive loops of Co and Ni in the presence of the Im-IL additive are greater than those for the Im-IL-free baths. This result occurs due to formation of a protective layer on the metal deposit surfaces, which happens without changing the corrosion behavior of the surface.[58,74] In the case of the Co deposit, the corrosion behavior does not change due to the presence of the additive in the bath, S5a.† Diffusion behavior is clearly observed on the Ni film in the presence Im-IL. S5c and d† shows the compatible equivalent circuits used to extract the electrokinetic data listed in T4. The higher value of R_{ct} of 2184 Ω cm^2 for Im-IL at 1×10^{-5} M compared to 500.1 Ω cm^2 for the Im-IL-free bath indicates the adsorption of Im-IL onto the Co deposit surface. The Cu substrate shows a low R_{ct} due to the highly aggressive NaCl solution. As shown in T4, the Ni-coated Cu substrate revealed higher resistance with diffusion properties that can be ascribed to the formation of a porous protective layer at the metal/solution interface.[58,75] This is also associated with a decrease in CPE due to the adsorption of the additive molecules onto the metal surface. The presence of 1×10^{-5} M of Im-IL increased the resistivity of the Ni deposit in the NaCl solution from 7.26×10^3 kΩ cm^2 to 22.3×10^3 kΩ cm^2, which resulted from a protective layer on the electrode surface.

S6† shows the potentiodynamic polarization curves for (a) the Co and (b) Ni deposits on the Cu substrate in the absence and presence of 1×10^{-5} M Im-IL using a 3.5% NaCl solution. The corrosion current density (i_{corr}) and corrosion potential (E_{corr}) of the Co and Ni samples deposited without and with Im-IL were obtained from the analysis of the recorded Tafel lines and are listed in T4. As it can be observed from S6† and T4, the i_{corr} decreases and the E_{corr} is shifted to more negative potential values for both the Co and Ni samples in the presence 1×10^{-5} M Im-IL. This result indicates that the Co and Ni coatings from the Im-IL solution have an increased and better corrosion resistance compared to the Co and Ni coatings from the Im-IL-free solution.

4. Conclusion

A new ionic liquid 1-methyl-3-((2-oxo-2-(2,4,5 trifluorophenyl) amino)ethyl)-1*H*-imidazol-3-ium iodide (Im-IL) was used as an additive during Ni and Co electrodeposition from acidic sulfate and Watts baths, respectively. Im-IL in the appropriate concentration (1×10^{-4} M for Ni, 1×10^{-5} M for Co) showed a greater improvement in the surface morphology and corrosion resistance properties of the Ni deposit compared to the Co deposit. A substantial shift in the polarization curves toward more negative potentials was observed during the electrodeposition of Ni than Co in the presence of Im-IL. Cyclic voltammetric measurements showed an increase in the nucleation overpotential in the presence of Im-IL, which indicated the inhibition of the Ni and Co electrodeposition process due to the adsorption of Im-IL ions on the cathode surface. The adsorption of Im-IL ions on the cathode surface during Ni and Co electrodeposition obeyed Langmuir adsorption. Im-IL led to the formation of a fine-grained and more compact deposit due to the inhibition of the ions of both metals during deposition, as shown by SEM and AFM studies. X-ray diffraction spectra revealed that the addition of Im-IL did not change the crystal structure of either of the electrodeposited metals. The CCE% of electrodeposition of both metals was very high (nearly 100%). From corrosion studies, a higher corrosion resistance of the Ni film than the Co film following deposition in the presence of 1×10^{-5} M Im-IL was inferred.

Conflicts of interest

There are no conflicts to declare.

References

1 M. A. M. Ibrahim and R. M. Al Radadi, Noncrystalline cobalt coatings on copper substrates by electrodeposition from complexing acidic glycine baths, *Mater. Chem. Phys.*, 2015, **151**, 222–232.
2 R. Fukui, Y. Katayama and T. Miura, The effect of organic additives in electrodeposition of Co from an amide-type ionic liquid, *Electrochim. Acta*, 2011, **56**(3), 1190–1196.
3 T. M. Manhabosco and I. L. Müller, Influence of saccharin on morphology and properties of cobalt thin films electrodeposited over n-Si (100), *Surf. Coat. Technol.*, 2008, **202**(15), 3585–3590.
4 S. S. A. El Rehim, M. A. M. Ibrahim and M. M. Dankeria, Electrodeposition of cobalt from gluconate electrolyte, *J. Appl. Electrochem.*, 2002, **32**(9), 1019–1027.
5 R. M. A. Radadi and M. A. M. Ibrahim, Nickel-cobalt alloy coatings prepared by electrodeposition Part I: Cathodic current efficiency, alloy composition, polarization behavior and throwing power, *Korean J. Chem. Eng.*, 2020, **37**(2), 1–10.
6 Z. Feng, L. Wang, D. Li, Q. Sun, P. Lu, P. Xing, *et al.*, Electrodeposition of Ni-Se in a chloride electrolyte: An

insight of diffusion and nucleation mechanisms, *J. Electroanal. Chem.*, 2019, **847**, 113195.

7 R. M. Al Raddadi. *Cathodic codeposition of nickel-cobalt alloy coatings from acidic glycine complex baths*, 2014.

8 Y.-J. Chang, S.-Z. Chen and C.-Y. Ho, Crystallographic structure of Ni–Co coating on the affinity adsorption of histidine-tagged protein, *Colloids Surf., B*, 2015, **128**, 55–60.

9 B. Bozzini and L. D'Urzo, An in-situ SERS Study of the Interfacial Behaviour of Coumarin During the Electrodeposition of Cobalt, *Int. J. Electrochem. Sci.*, 2009, **4**, 1028–1051.

10 Q. S. Jiang, W. Cheng, W. Li, Z. Yang, Y. Zhang, R. Ji, *et al.*, One-step electrodeposition of amorphous nickel cobalt sulfides on FTO for high-efficiency dye-sensitized solar cells, *Mater. Res. Bull.*, 2019, **114**, 10–17.

11 J. Wojciechowski, M. Baraniak, J. Pernak and G. Lota, Nickel Coatings Electrodeposited from Watts Type Baths Containing Quaternary Ammonium Sulphate Salts, *Int. J. Electrochem. Sci.*, 2017, 3350–3360.

12 M. A. M. Ibrahim and R. M. Al Radadi, Role of glycine as a complexing agent in nickel electrodeposition from acidic sulphate bath, *Int. J. Electrochem. Sci.*, 2015, **10**(6), 4946.

13 E. P. S. Schmitz, S. P. Quinaia, J. R. Garcia, C. K. de Andrade and M. C. Lopes, Influence of commercial organic additives on the nickel electroplating, *Int. J. Electrochem. Sci.*, 2016, **11**, 983–997.

14 N. F. El Boraei and M. A. M. Ibrahim, Catalytic effect of l-proline on the reduction of Ni (II) ions during nickel electrodeposition from a Watts-type nickel bath, *Surf. Coat. Technol.*, 2018, **347**, 113–122.

15 K. M. Sivaraman, O. Ergeneman, S. Pané, E. Pellicer, J. Sort, K. Shou, *et al.*, Electrodeposition of cobalt–yttrium hydroxide/oxide nanocomposite films from particle-free aqueous baths containing chloride salts, *Electrochim. Acta*, 2011, **56**(14), 5142–5150.

16 L. Tian, J. Xu and S. Xiao, The influence of pH and bath composition on the properties of Ni–Co coatings synthesized by electrodeposition, *Vacuum*, 2011, **86**(1), 27–33.

17 S. S. Abd El Rehim, M. A. M. Ibrahim, M. M. Dankeria and M. Emad, Electrodeposition of amorphous cobalt-manganese alloys on to steel from gluconate baths, *Trans. IMF*, 2002, **80**(3), 105–109.

18 G. Nemţoi, H. Chiriac, O. Dragoş, M.-O. Apostu and D. Lutic, The voltammetric characterization of the electrodeposition of cobalt, nickel and iron on gold disk electrode, *Acta Chem. Iasi*, 2009, **17**, 151–168.

19 S. S. Abd El Rehim, S. M. Abd El Wahaab, M. A. M. Ibrahim and M. M. Dankeria, Electroplating of cobalt from aqueous citrate baths, *J. Chem. Technol. Biotechnol.*, 1998, **73**(4), 369–376.

20 C. A. Loto, Electrodeposition of zinc from acid based solutions: a review and experimental study, *Asian J. Appl. Sci.*, 2012, **5**(6), 314–326.

21 H. El-Feky, M. Negem, S. Roy, N. Helal and A. Baraka, Electrodeposited Ni and Ni-Co alloys using cysteine and conventional ultrasound waves, *Sci. China: Chem.*, 2013, **56**(10), 1446–1454.

22 J. Guo, X. Guo, S. Wang, Z. Zhang, J. Dong, L. Peng, *et al.*, Effects of glycine and current density on the mechanism of electrodeposition, composition and properties of Ni–Mn films prepared in ionic liquid, *Appl. Surf. Sci.*, 2016, **365**, 31–37.

23 S. Wang, X. Guo, H. Yang, J. Dai, R. Zhu, J. Gong, *et al.*, Electrodeposition mechanism and characterization of Ni–Cu alloy coatings from a eutectic-based ionic liquid, *Appl. Surf. Sci.*, 2014, **288**, 530–536.

24 X. Ji, C. Yan, H. Duan and C. Luo, Effect of phosphorous content on the microstructure and erosion–corrosion resistance of electrodeposited Ni-Co-Fe-P coatings, *Surf. Coat. Technol.*, 2016, **302**, 208–214.

25 Y.-L. Zhu, Y. Katayama and T. Miura, Effects of coumarin and saccharin on electrodeposition of Ni from a hydrophobic ionic liquid, *Electrochim. Acta*, 2014, **123**, 303–308.

26 M. Zamani, A. Amadeh and S. M. L. Baghal, Effect of Co content on electrodeposition mechanism and mechanical properties of electrodeposited Ni–Co alloy, *Trans. Nonferrous Met. Soc. China*, 2016, **26**(2), 484–491.

27 G. Cârâc and A. Ispas, Effect of nano-Al2O3 particles and of the Co concentration on the corrosion behavior of electrodeposited Ni–Co alloys, *J. Solid State Electrochem.*, 2012, **16**(11), 3457–3465.

28 M. H. Allahyarzadeh, B. Roozbehani and A. Ashrafi, Electrodeposition of high Mo content amorphous/nanocrystalline Ni–Mo alloys using 1-ethyl-3-methyl-imidazolium chloride ionic liquid as an additive, *Electrochim. Acta*, 2011, **56**(27), 10210–10216.

29 P. Yang, Y. Zhao, C. Su, K. Yang, B. Yan and M. An, Electrodeposition of Cu–Li alloy from room temperature ionic liquid 1-butyl-3-methylimidazolium tetrafluoroborate, *Electrochim. Acta*, 2013, **88**, 203–207.

30 C. Lupi, A. Dell'Era and M. Pasquali, Effectiveness of sodium citrate on electrodeposition process of NiCoW alloys for hydrogen evolution reaction, *Int. J. Hydrogen Energy*, 2017, **42**(48), 28766–28776.

31 E. M. Oliveira, G. A. Finazzi and I. A. Carlos, Influence of glycerol, mannitol and sorbitol on electrodeposition of nickel from a Watts bath and on the nickel film morphology, *Surf. Coat. Technol.*, 2006, **200**(20–21), 5978–5985.

32 Z. Jamil, E. Ruiz-Trejo and N. P. Brandon, Nickel Electrodeposition on Silver for the Development of Solid Oxide Fuel Cell Anodes and Catalytic Membranes, *J. Electrochem. Soc.*, 2017, **164**(4), D210–D217.

33 J. Deng, J. Zhang, Y. Tu, P. Yang, M. An and P. Wang, Effect of BEO in the electrodeposition process of Ni/diamond composite coatings for preparation of ultra-thin dicing blades: Experiments and theoretical calculations, *Ceram. Int.*, 2018, **44**(14), 16828–16836.

34 H. F. Alesary, S. Cihangir, A. D. Ballantyne, R. C. Harris, D. P. Weston, A. P. Abbott, *et al.*, Influence of additives on

the electrodeposition of zinc from a deep eutectic solvent, *Electrochim. Acta*, 2019, **304**, 118–130.

35 M. Tomie, T. Akita, M. Irita and M. Hayase, Transitional Additive Adsorption with Co-Addition of Suppressor and Leveler for Copper TSV Filling, *J. Electrochem. Soc.*, 2012, **167**(8), 82513.

36 S. Hamilakis, D. Balgis, K. Milonakou-Koufoudaki, C. Mitzithra, C. Kollia and Z. Loizos, Electrodeposition of CdSe photoabsorber thin films in the presence of selected organic additives, *Mater. Lett.*, 2015, **145**, 11–14.

37 A. B. Hashemi, G. Kasiri and F. La Mantia, The effect of polyethyleneimine as an electrolyte additive on zinc electrodeposition mechanism in aqueous zinc-ion batteries, *Electrochim. Acta*, 2017, **258**, 703–708.

38 U. S. Mohanty, B. C. Tripathy, P. Singh and S. C. Das, Effect of Cd2+ on the electrodeposition of nickel from sulfate solutions. Part I: Current efficiency, surface morphology and crystal orientations, *J. Electroanal. Chem.*, 2002, **526**(1–2), 63–68.

39 Y.-L. Zhu, Y. Katayama and T. Miura, Effects of acetone and thiourea on electrodeposition of Ni from a hydrophobic ionic liquid, *Electrochim. Acta*, 2012, **85**, 622–627.

40 M. A. M. Ibrahim and E. M. A. Omar, Synergistic effect of ninhydrin and iodide ions during electrodeposition of zinc at steel electrodes, *Surf. Coat. Technol.*, 2013, **226**, 7–16.

41 Z. Qibo and H. Yixin, Ionic Liquids as Electrodeposition Additives and Corrosion Inhibitors, in *Progress and Developments in Ionic Liquids*, InTech, 2017.

42 K. Yao, M. Zhai and Y. Ni, α-Ni(OH)2·0.75 H2O nanofilms on Ni foam from simple NiCl2 solution: Fast electrodeposition, formation mechanism and application as an efficient bifunctional electrocatalyst for overall water splitting in alkaline solution, *Electrochim. Acta*, 2019, **301**, 87–96.

43 S. Ibrahim, A. Bakkar, E. Ahmed and A. Selim, Effect of additives and current mode on zinc electrodeposition from deep eutectic ionic liquids, *Electrochim. Acta*, 2016, **191**, 724–732.

44 L. Anicai, A. Florea and T. Visan, Studies regarding the nickel electrodeposition from choline chloride based ionic liquids, in *Applications of Ionic Liquids in Science and Technology*, InTech, 2011.

45 Y. Song, J. Tang, J. Hu, H. Yang, W. Gu, Y. Fu, *et al.*, Interfacial assistant role of amine additives on zinc electrodeposition from deep eutectic solvents: an in situ X-ray imaging investigation, *Electrochim. Acta*, 2017, **240**, 90–97.

46 S. Costovici, A.-C. Manea, T. Visan and L. Anicai, Investigation of Ni-Mo and Co-Mo alloys electrodeposition involving choline chloride based ionic liquids, *Electrochim. Acta*, 2016, **207**, 97–111.

47 A. S. Ismail, Electrodeposition of aluminium–copper alloy from 1-butyl-1-methylpyrrolidinium bis (trifluoromethylsulfonyl) imide ionic liquid, *Egypt. J. Pet.*, 2017, **26**(1), 61–65.

48 R. Mardani, H. Shahmirzaee, H. Ershadifar and M. R. Vahdani, Electrodeposition of Ni32Fe48Mo20 and Ni52Fe33W15 alloy film on Cu microwire from ionic liquid containing plating bath, *Surf. Coat. Technol.*, 2017, **324**, 281–287.

49 Y. Sun, Z. Wang, Y. Wang, M. Liu, S. Li, L. Tang, *et al.*, Improved transport of gold (I) from aurocyanide solution using a green ionic liquid-based polymer inclusion membrane with in-situ electrodeposition, *Chem. Eng. Res. Des.*, 2020, **153**, 136–145.

50 A. Bakkar and V. Neubert, Electrodeposition of photovoltaic thin films from ionic liquids in ambient atmosphere: Gallium from a chloroaluminate ionic liquid, *J. Electroanal. Chem.*, 2020, **856**, 113656.

51 N. Rezki, F. F. Al-blewi, S. A. Al-Sodies, A. K. Alnuzha, M. Messali, I. Ali, *et al.*, Synthesis, Characterization, DNA Binding, Anticancer, and Molecular Docking Studies of Novel Imidazolium-Based Ionic Liquids with Fluorinated Phenylacetamide Tethers, *ACS Omega*, 2020.

52 M. A. El Sayed and M. A. M. Ibrahim, Natural Kermes Dye as an Effective Additive for Electrochemical Deposition of Nickel from Watts-type Nickel Bath, *Int. J. Electrochem. Sci.*, 2019, **14**, 4957–4973.

53 F. Lallemand, D. Comte, L. Ricq, P. Renaux, J. Pagetti, C. Dieppedale, *et al.*, Effects of organic additives on electroplated soft magnetic CoFeCr films, *Appl. Surf. Sci.*, 2004, **225**(1–4), 59–71.

54 U. P. Kumar, S. Shanmugan, C. J. Kennady and S. M. A. Shibli, Anti-corrosion and microstructural properties of Ni–W alloy coatings: effect of 3, 4-Dihydroxybenzaldehyde, *Heliyon*, 2019, **5**(3), e01288.

55 S. Ren, Z. Lei and Z. Wang, Investigation of nitrogen heterocyclic compounds as levelers for electroplating cu filling by electrochemical method and quantum chemical calculation, *J. Electrochem. Soc.*, 2015, **162**(10), D509–D514.

56 N. Sorour, W. Zhang, E. Ghali and G. Houlachi, A review of organic additives in zinc electrodeposition process (performance and evaluation), *Hydrometallurgy*, 2017, **171**, 320–332.

57 Q. Zhang and Y. Hua, Kinetic investigation of zinc electrodeposition from sulfate electrolytes in the presence of impurities and ionic liquid additive [BMIM] HSO4, *Mater. Chem. Phys.*, 2012, **134**(1), 333–339.

58 A. M. Al-Fakih, H. H. Abdallah and M. Aziz, Experimental and theoretical studies of the inhibition performance of two furan derivatives on mild steel corrosion in acidic medium, *Mater. Corros.*, 2019, **70**(1), 135–148.

59 M. Gholami, I. Danaee, M. H. Maddahy and M. RashvandAvei, Correlated ab initio and electroanalytical study on inhibition behavior of 2-mercaptobenzothiazole and its thiole–thione tautomerism effect for the corrosion of steel (API 5L X52) in sulphuric acid solution, *Ind. Eng. Chem. Res.*, 2013, **52**(42), 14875–14889.

60 M. A. M. Ibrahim and M. Messali, Ionic Liquid [BMPy] Br as an effective additive auring Zinc electrodeposition from an aqueous Sulfate bath, *Prod. Finish.*, 2011, **2**, 14.

61 F. F. Huang and M. L. Huang, Complexation Behavior and Co-Electrodeposition Mechanism of Au-Sn Alloy in Highly Stable Non-Cyanide Bath, *J. Electrochem. Soc.*, 2018, **165**(3), D152–D159.

62 R. P. Oliveira, D. C. Bertagnolli, E. A. Ferreira, L. da Silva and A. S. Paula, Influence of Fe2+ oxidation and its antioxidant ascorbic acid as additive in Zn-Ni-Fe electrodeposition process on a low carbon steel, *Surf. Coat. Technol.*, 2018, **349**, 874–884.

63 A. Abebe, S. Admassie, I. J. Villar-Garcia and Y. Chebude, 4, 4-Bipyridinium ionic liquids exhibiting excellent solubility for metal salts: Potential solvents for electrodeposition, *Inorg. Chem. Commun.*, 2013, **29**, 210–212.

64 S. Saha, S. Sultana, M. M. Islam, M. M. Rahman, M. Y. A. Mollah and M. A. B. H. Susan, Electrodeposition of cobalt with tunable morphology from reverse micellar solution, *Ionics*, 2014, **20**(8), 1175–1181.

65 M. A. Ibrahim and R. S. Bakdash, New cyanide-free ammonia bath for brass alloy coatings on steel substrate by electrodeposition, *Int. J. Electrochem. Sci.*, 2015, **10**, 9666–9677.

66 T. R. Copeland and R. K. Skogerboe, Anodic stripping voltammetry, *Anal. Chem.*, 1974, **46**(14), 1257A–1268a.

67 M. A. M. Ibrahim, S. S. A. El Rehim, S. M. A. El Wahaab and M. M. Dankeria, Nickel electroplating on steel from acidic citrate baths, *Plat. Surf. Finish.*, 1999, **86**(4), 69–75.

68 W. Wu, N. Eliaz and E. Gileadi, Electrodeposition of Re-Ni alloys from aqueous solutions with organic additives, *Thin Solid Films*, 2016, **616**, 828–837.

69 J. Wang, Y. Wang, T. Xie and Q. Deng, Facile and fast synthesis of Ni composite coating on Ti mesh by electrodeposition method for high-performance hydrogen production, *Mater. Lett.*, 2019.

70 N. M. Pereira, O. Brincoveanu, A. G. Pantazi, C. M. Pereira, J. P. Araujo, A. F. Silva, *et al.*, Electrodeposition of Co and Co composites with carbon nanotubes using choline chloride-based ionic liquids, *Surf. Coat. Technol.*, 2017, **324**, 451–462.

71 Z. Feng, D. Li, Q. Sun, L. Wang, P. Xing and M. An, Insight into the role and mechanism of 2, 2-bipyridine as a novel additive for nano-electrodeposition of Zn-Ni alloy, *J. Alloys Compd.*, 2018, **765**, 1026–1034.

72 H. Rahal, R. Kihal, A. M. Affoune and S. Rahal, Electrodeposition and characterization of Cu2O thin films using sodium thiosulfate as an additive for photovoltaic solar cells, *Chin. J. Chem. Eng.*, 2018, **26**(2), 421–427.

73 A. K. Al-Harbi and K. M. Emran, Effect of immersion time on electrochemical and morphology of new Fe-Co metal-metal glassy alloys in acid rain, *Arabian J. Chem.*, 2019, **12**(1), 134–141.

74 K. M. Emran and H. AL-Refai, Electrochemical and surface investigation of Ni-Cr glassy alloys in nitric acid solution, *Int. J. Electrochem. Sci.*, 2017, **12**, 6404–6416.

75 A. Bahramian, M. Eyraud, F. Vacandio and P. Knauth, Improving the corrosion properties of amorphous Ni-P thin films using different additives, *Surf. Coat. Technol.*, 2018, **345**, 40–52.

